# Active material blending strategy improves the comprehensive performance of electrode:A case study

Wei Li [a],[1], Yuan Qin [a],[1], Shini Lin [a], Honghao Xie [a], Jing Zeng [a],[**], Peng Zhang [b],[***], Jinbao Zhao [a],[*]

[a] State-Province Joint Engineering Laboratory of Power Source Technology for New Energy Vehicle, State Key Laboratory of Physical Chemistry of Solid Surfaces, Engineering Research Center of Electrochemical Technology, Collaborative Innovation Center of Chemistry for Energy Materials, Ministry of Education, College of Chemistry and Chemical Engineering, Xiamen University, Xiamen, 361005, China
[b] College of Energy & School of Energy Research, Xiamen University, Xiamen, 361102, China

## HIGHLIGHTS

- The comprehensive performance of electrode is improved through blending strategy.
- The blending strategy enhances battery energy density from multiple dimensions.
- The use of pilot equipment makes experimental results more reliable.

## GRAPHICAL ABSTRACT
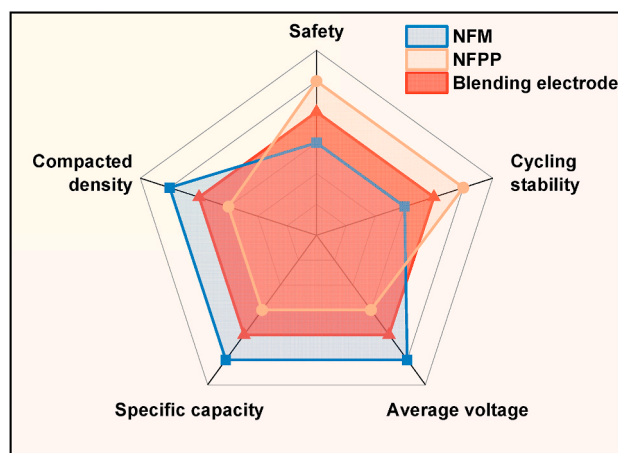
## ABSTRACT

In battery production, the comprehensive performance of cathode materials is the key to achieving applications. However, in the research area of cathode, their modification is limited to improving the material properties only from one or two aspects, mainly focused on doping, coating and other methods. Potentially, physical mixtures of multiple types of cathode materials with different characteristics is regarded as an effective strategy to enhance the comprehensive performance of batteries. In this work, cathode materials of $NaNi_{1/3}Fe_{1/3}Mn_{1/3}O_2$ (NFM) and $Na_4Fe_3(PO_4)_2(P_2O_7)$ (NFPP) will be used as a case model to investigate the improvement of battery performance by blended electrodes. And the pilot equipment is used throughout the entire manufacturing process of electrode

* Corresponding author.
** Corresponding author.
*** Corresponding author.
   E-mail addresses: zengjing@xmu.edu.cn (J. Zeng), pengzhang@xmu.edu.cn (P. Zhang), jbzhao@xmu.edu.cn (J. Zhao).
[1] These authors contributed equally to this work.

to ensure that the experimental results are closer to practical production. After analyzing from multiple angles, we discover that the blended electrodes compensate for the shortcomings of single electrodes, thereby effectively improving their overall performance; at the same time, it comprehensively improves the energy density of the battery in multiple dimensions such as electrode characteristics and electrochemical performance. These significant improvement effects are difficult to achieve solely through material modification. This work shows that active material blending strategy is a promising approach to improve the general performance of SIBs.

## 1. Introduction

Under the pressures of environmental pollution and energy crisis, the applications of clean energy and large-scale energy storage are receiving increasing attention[1–3]. Sodium-ion batteries (SIBs) have become the preferred technology for large-scale energy storage due to their abundant resources and excellent performance [4,5]. SIBs are hoped to become a supplement to lithium-ion batteries (LIBs) and reduce excessive consumption of limited lithium resources [6,7]. In recent years, a large amount of researches have promoted the continuous improvement of energy density, cycling stability and safety of SIBs, further propelling its application in energy storage products [8,9].

In the research of SIBs, the cathode material is considered to be the key to improving battery performance due to the stability of crystal structure and the limitation of electron transfer number [10]. For cathode materials, research work mainly focuses on layer and tunnel type transition metal oxides, polyanionic materials, Prussian blue analogues and organic compounds [11,12]. The main advantages of transition metal layered oxide cathode materials are high theoretical specific capacity and high compaction density[13–15], but there are also difficulties in poor cycling stability and thermal stability. Among diverse polyanionic materials, iron-based phosphate has garnered significant interest for commercialization on account of its stable structure and long cycle performance. Unfortunately, the low energy density reduces its competitiveness [16,17]. Developing cathode materials with excellent comprehensive performance is an important way to promote the large-scale application of SIBs.

Various modification methods have been adopted to improve the performance of different cathode materials due to their shortcomings. For polyanionic materials with low theoretical capacity, Xia et al. [18] introduced reduced graphene oxide during the synthesis of NFPP, resulting in an initial reversible specific capacity of 110.2 mAh g$^{-1}$ at 0.1C for the composite cathode. In addition, Ma et al. [19] improved the intrinsic conductivity of the material by doping with $Gr^{3+}$, effectively promoting the migration of sodium ions during charge and discharge processes. The initial capacity of the modified material at 0.1C was 113.6 mAh g$^{-1}$. However, due to the theoretical specific capacity of NFPP being only 129 mAh g$^{-1}$, the space for capacity improvement is restricted. The NaNi$_{1/3}$Fe$_{1/3}$Mn$_{1/3}$O$_2$ (NFM) materials with high specific capacity, has a disadvantage of poor cycling stability. Many strategies were used to improve its cycling stability, but with little effect [20]. Compare to traditional modification, cathode materials blending strategy has been proven to as a promising approach to improve the comprehensive performance [21,22]. Nevertheless, the strategy is often overlooked in scientific research. In long-term research and industrial production, blended strategy of cathode materials has been proven to have the advantages of low cost and repeatable preparation process [23]. And the physical and chemical characteristics of the blended materials mainly depend on the proportion of each component materials, which play a significant role in the battery voltage, capacity, rate and cycle performance, tap density, compacted density, safety performance, as well as energy density[24–26].

In this work, NFM and NFPP were mixed in different proportions in planetary triple high-speed disperse mixer to produce blended electrode, which were used as a case for subsequent research. The improvement of the comprehensive performance of blended electrodes were systematically studied from multiple perspectives, including electrode characteristics, electrochemical performance, and thermal stability. Research has found that blended electrodes have general optimization for whether the compaction density, the electrolyte absorption rate, or the specific capacity, thereby significantly improving the energy density of the battery compared with NFPP. In terms of NFM, the performance of blended electrodes effectively optimized in multiple aspects, include cycling stability, kinetic properties and heat release. Through blending strategies, the comprehensive performance of materials can be conveniently and effectively improved, which will provide effective support for the development of low-cost, high-energy density, and high-safety SIBs.

## 2. Material and methods

### 2.1. Electrode preparation

The cathode materials NaNi$_{1/3}$Fe$_{1/3}$Mn$_{1/3}$O$_2$ (NFM) and Na$_3$Fe$_2$PO$_4$P$_2$O$_7$ (NFPP) are commercial materials. The cathodes slurry was prepared by mixing cathode material, Super P, Carbon nanotube (CNT) and polyvinylidene fluoride (PVDF) binder with a mass ratio of 94.5:2:0.5:3.0 in N-methyl-2-pyrrolidone (NMP). Then, the cathode slurry was coated on carbon coated Al foils. Finally, the electrodes were dried at 80 °C in vacuum for 12 h. The active mass loadings of the cathode were about 12.0–13.0 mg cm$^{-2}$. The entire experimental process was conducted using pilot equipment, including planetary triple high-speed dispersion mixer, high precision coating device, and high precision battery plating roller (Optical images are shown in Fig. S1).

### 2.2. Material characterization

The crystallographic structure of the specimens was determined utilizing X-ray diffraction analysis (Rigaku Miniflex 600 instrument), with a scan rate of 5° per minute and employing Cu Kα radiation. The surface morphologies of the samples were characterized through the scanning electron microscopy (SEM, Hitachi S-4800). Furthermore, the differential scanning calorimetry-thermogravimetry-mass spectrometry (DSC-TG-MS, SDT-650 + Discovery MS) was to analyze the thermal behavior of samples in a temperature range of 50–400 °C with a heat rate of 5 °C min$^{-1}$.

### 2.3. Electrochemical measurements

All cells were assembled using the 2016-type coin cell. In addition, glass fibers (GF/D, Whatman), a counter electrode (Na metal sheet), and electrolyte (Hunan Fenlanite New Energy Technology Co., Ltd.) were also used for battery assembly. All the assembly processes were operated in a glove box filled with argon (H$_2$O, O$_2$ < 0.5 ppm). The specific capacity was calculated based on the total mass weight of NFM and NFPP in the blended electrode. Galvanostatic charge and discharge (GCD) test was conducted on the Neware battery test system with a voltage range of 1.5–4.0 V (vs Na$^+$/Na) at room temperature. What's more, the galvanostatic intermittent titration technique (GITT) was performed on the LAND battery testing system in a voltage range of 1.5–4.0 V. The cells were charged at 0.1C for 10 min, followed by open-circuit relaxation of 1 h. The current values of various rates were calculated according to the specious capacity of NFM (120 mAh g$^{-1}$) and NFPP (105 mAh g$^{-1}$). All electrochemical tests were carried out at the room temperature.

## 3. Results and discussion

In order to ensure that the experimental results are more closely related to practical applications, the pilot equipment is used throughout the entire electrode manufacturing process. Firstly, the active material, conductive agent, binder, CNT, and NMP were thoroughly mixed in the planetary triple high-speed dispersion mixer (about 6 h). Then, the slurry was conducted a qualification test using a viscometer and particle size analyzer. If it fails, continue stirring until it meets the requirements (sometimes NMP needs to be added again). Subsequently, we filtered the qualified slurry. Finally, coating, electrode baking, and electrode rolling processes were carried out. It is worth noting that the above operations must be carried out in a dry environment to prevent the active materials from deteriorating. The specific process diagram is shown in Fig. 1, and the experimental record is shown in Figs. S2 and S3. All subsequent experiments and tests were conducted using the electrode prepared by this process.

The XRD patterns of different mixed ratios of NFM and NFPP are shown in Fig. 2(a). The lattice spacing differences are chiefly reflected in the diffraction peaks of NFM at diffraction angles of 16° and 41°, with the peak intensity being directly proportional to the content of NFM. This indicates that the composition of the blended electrode is rational. Moreover, no new peaks were observed in XRD after mixing, indicating that there were no side reactions. NFM and NFPP were initially measured in the Laser particle size analyzer and SEM (Fig. 2(b), Figure S4), The particle size distribution of NFPP predominantly ranging from 1 to 10 μm. And the powder of NFM exhibits a normal distribution in particle size, predominantly within the range of 5–10 μm. The median particle sizes ($D_{50}$) of NFM and NFPP are 10.675 μm and 6.848 μm. After mixing larger particle size NFM with smaller particle size NFPP, a morphology of small particles filling pores and large particle gaps is observed (Fig. 2(c)). Through SEM and mapping images of elements, it can be observed that the large particles of NFM and the small particles of NFPP in the blended electrode are uniformly mixed. Subsequent

research based on this blended electrode is reliable (Fig. 2(d and e)). Additionally, a detailed study was conducted on the basic characteristics of blended electrode (compaction density, electrolyte absorption rate and so on). Tap density and compaction density are important indicators for measuring the compactness of materials and play a crucial role in improving the energy density of batteries, and the testing method for compaction density is shown in Fig. S5. The tap density and compaction density of NFM are 1.73 g/cm$^3$ and 3.02 g/cm$^3$, respectively, while those of NFPP are only 1.12 g/cm$^3$ and 2.00 g/cm$^3$. Compared to NFPP, the compaction density of the blended cathode has been significantly improved (Fig. 2(f)–Table S1). It is worth noting that the growth rates of compacted density and tap density are not consistent, which may be due to the influence of particle size distribution on the physical properties of the electrode. Additionally, the electrolyte absorption rate of NFPP is higher than that of NFM. With the increase of NFM blending ratio, the electrolyte absorption rate of the blended cathode will also decrease linearly (Fig. 2(g)). Compared to NFPP, the increase in compaction density and the decrease in electrolyte absorption rate of the blended cathode both contribute to the improvement of battery energy density.

Subsequently, the electrochemical performance of the blended electrode was further studied. The mixed cathode is subjected to capacity testing in the voltage range of 1.5–4.0 V and at a rate of 0.1/1.0C. The capacity of the blended cathode has been significantly improved (compared with NFPP), and shows a linear growth relationship with the amount of NFM added. The fitting curve of capacity change of 0.1/1.0C conforms to the equation y = 21.53*x+105.05, y = 22.37*x+96.31 (x is the proportion of NFM added, 0<x < 100) (Fig. 3(a and b)). More detailed capacity information can be found in Table S2. The different slopes of the fitting curve can also provide data references for electrode design in different usage scenario. The increase in the proportion of NFM significantly enhances the specific capacity of the battery. Furthermore, we normalized the voltage-capacity curve of the first charge and discharge cycle (Fig. S6). Due to the different oxidation-reduction reactions that occur when the cathode material gains and loses electrons,
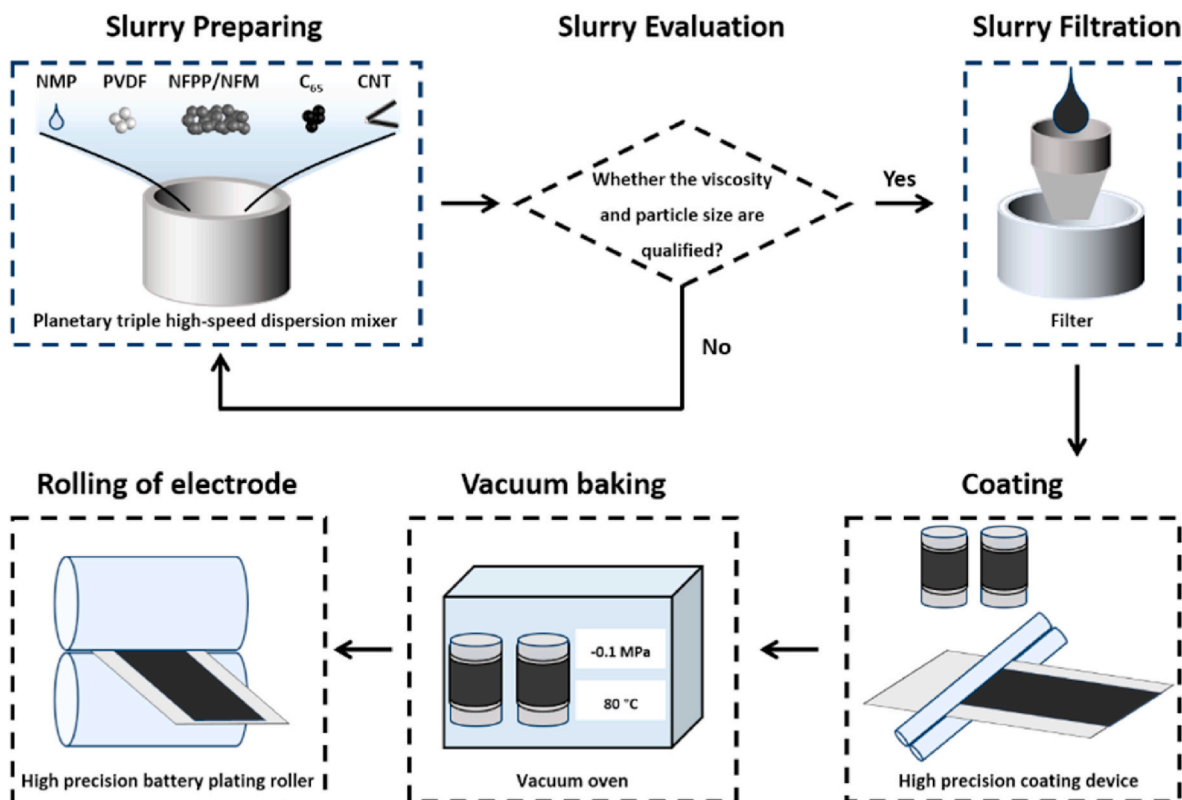


**Fig. 1.** Schematical illustrations of the preparations of the battery slurries and electrodes.
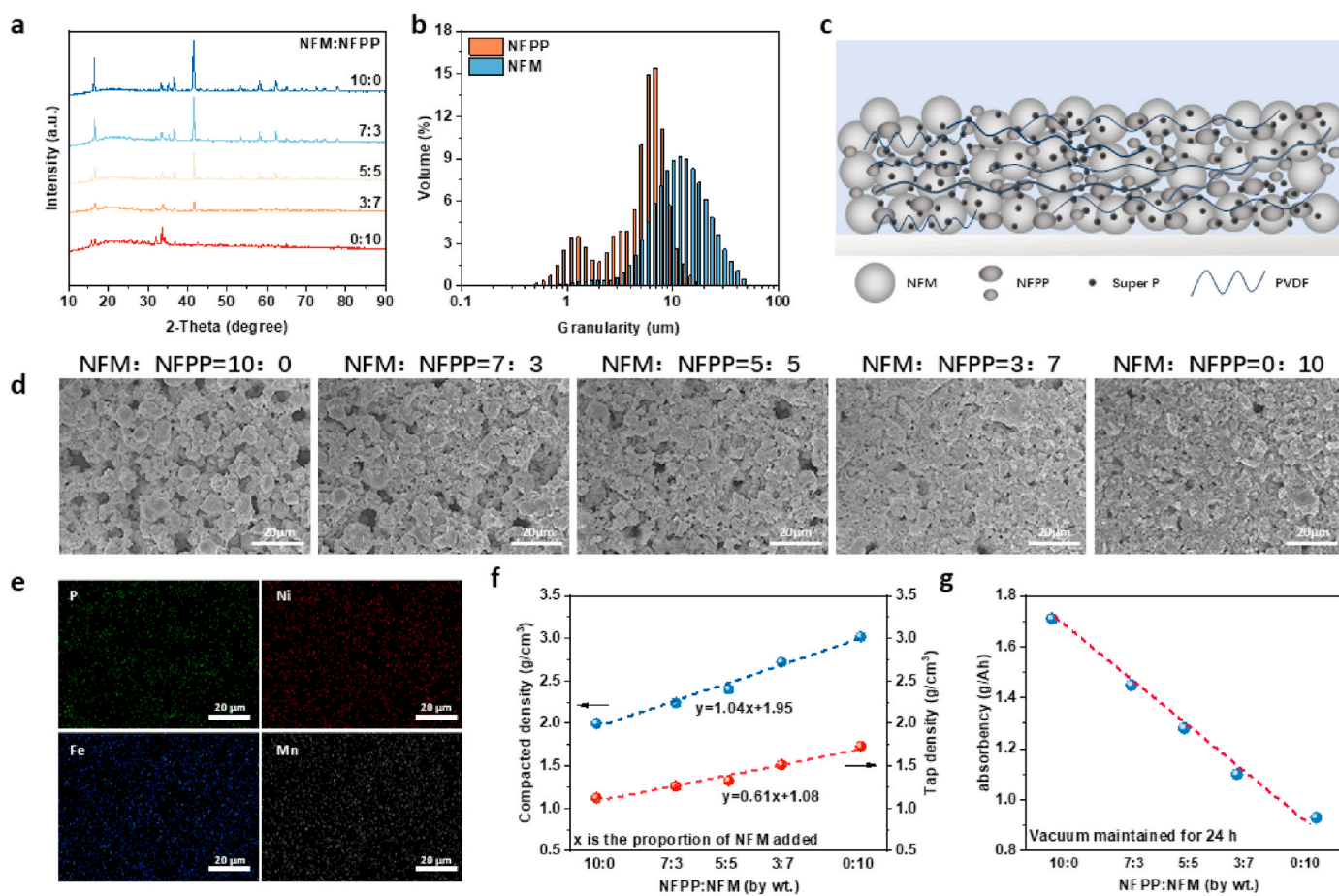
**Fig. 2.** Physical characteristics and properties of blended electrode. (a) The x-ray diffraction patterns of different mixed ratios of NFM and NFPP; (b) The particle size distribution of NFPP and NFM; (c) Schematic illustration of the materials distribution of blended electrode; (d) SEM images of NFM-NFPP electrode mixed in different proportions for 10:0, 7:3, 5:5, 3:7, 0:10; (e) Mapping images of elements (P, Ni, Fe, and Mn); (f) Linear relationship graph between tap density and compacted density; (g) electrolyte absorption rate, and the blended proportions of NFM-NFPP.

there are significant differences in the voltage plateau during the charge and discharge process. The differential capacity (dQ/dV) curve also illustrates this point (Fig. 3(c)). In the study of NFM material, the anodic oxidation peaks observed at 2.8 V and 3.6 V are attributed to the redox couples of $Ni^{2+}/N^{3+}$ and $Ni^{3+}/Ni^{4+}$, respectively [27]. The capacity contribution of NFPP originates from the reversible redox transition of $Fe^{2+}/Fe^{3+}$ [16]. Concurrently, this transition prompts the extraction of $Na^+$ ions from various crystallographic sites, thereby generating two distinct oxidation peaks as observed in Fig. 3(c). The oxidation peak at 2.75 V is corresponding to the extraction of $Na^+$ at Na3 (5-coordinated) and Na1 (6-coordinated) with the extraction of and sites [28]. In addition, the oxidation peaks at 3.20 V are assigned to the transformation of $Na^+$ at Na4 site (6-coordinated) [29]. In addition to the increase in capacity, the increase in discharge platform voltage of the blended cathode will also contribute to the improvement of energy density. When the charging and discharging voltage range is extended to 1.5–4.3 V, the increase in discharge capacity also shows a linear growth pattern, and the fitting curve of capacity change conforms to the equation y = 54.43*x+104.73 (x is the doping ratio of NFM, 0<x < 100) (Fig. 3(d and e)). Under high voltage cycling, the capacity growth rate of the mixed electrode doubles, due to the emergence of a new platform for NFM above 4.0 V (Fig. 3(f)).

According to the above experimental data, we normalized the discharge curve based on the discharge capacity and calculated the average voltage during the discharge process through integration. The average discharge voltages of NFPP and NFM were calculated to be 2.92 V and 3.09 V, respectively. At the same time, the average voltage of the

blended cathode showed a linear increasing trend (Figure S7, Fig. 4(a)). Subsequently, based on the average voltage, cathode capacity, and cell design parameters, the variation trend of the energy density (mass energy density and volume energy density) of the blended electrodes was roughly estimated (Fig. 4(b and c)). The estimated results are based on the cell design parameters in Table S3 and Table S4. The increase in energy density of the entire battery is not only related to the capacity of the cathode material, but also to the average discharge voltage, the compaction density of the cathode material, as well as the electrolyte absorption rate of the electrode. Nevertheless, the common modification of cathode materials is limited to one or two aspects of improvement [30–34]. By contrast, the blending material strategy can effectively enhance the comprehensive performance of materials, thereby significantly improving the energy density of batteries (Fig. 4(d)).

The above analysis mainly indicates that the strategy of incorporating NFM into NFPP has achieved a significant increase in battery energy density. Reciprocally, the incorporation of NFPP will also improve the performance of NFM. NFM with high specific capacity is plagued by Jahn–Teller distortion in practical applications, leading to severe structure instability and capacity fade [20]. The blended electrode of structurally stable NFPP and NFM exhibit better cycling stability and slower energy density decay compared to NFM alone (Fig. 5(a and b)). Whether at a charging cut-off voltage of 4.0 V or 4.3 V, the cycling stability of the blended cathode has been significantly improved. And we found that increasing the cut-off voltage to 4.3 V does not deteriorate the performance of NFPP. In addition, when NFM is blended with NFPP, it has been demonstrated to significantly enhance the rate performance,
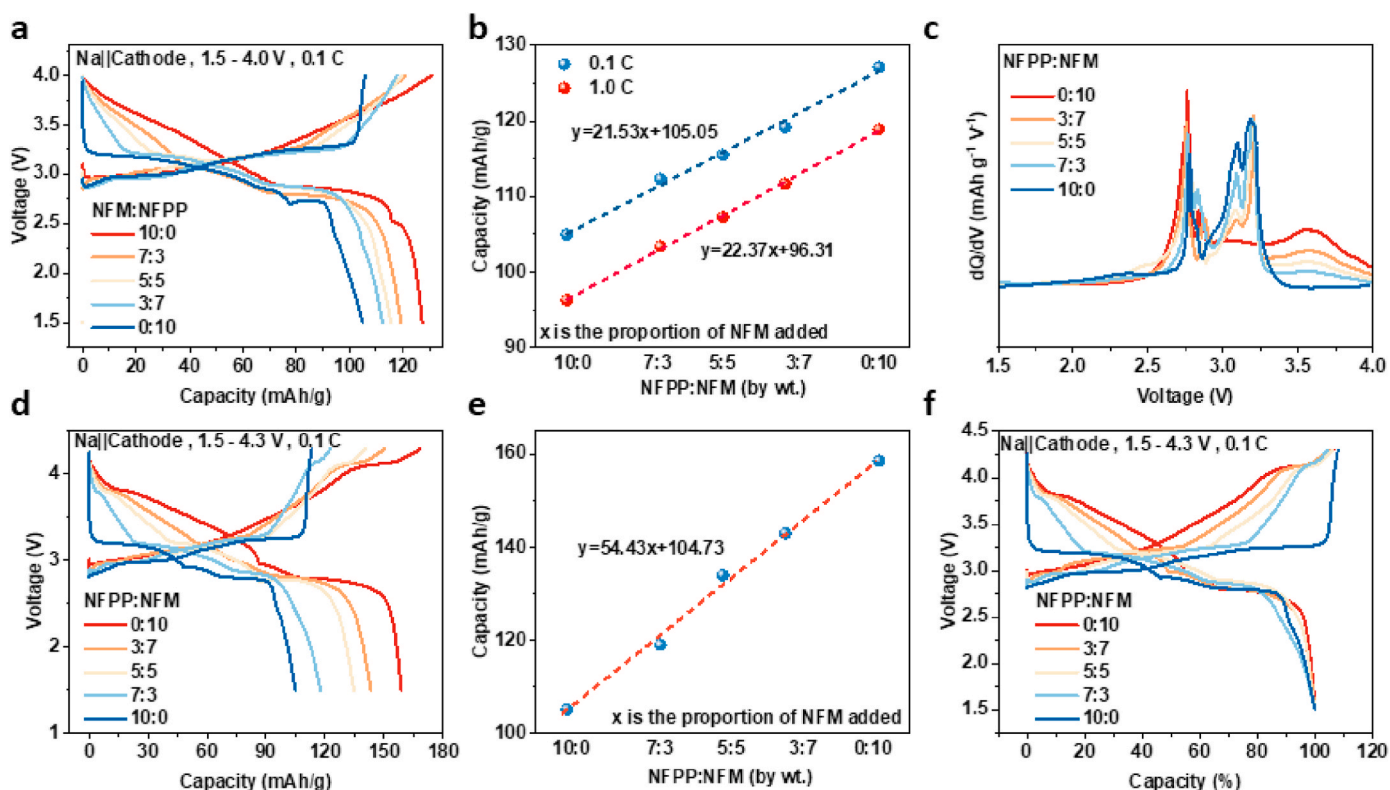
**Fig. 3.** Electrochemical performance of NFM-NFPP electrode blended by different proportions. (a) Initial charge-discharge curves of Na/NFM-NFPP full cells (1.5–4.0 V, 0.1C, 25 °C) in commercial electrolyte; (b) The relationship between capacity and NFPP electrode added by the amount of NFM at 0.1C, and 1C; (c) Corresponding dQ/dV curves of the charge process of (a); (d) First charge-discharge curves of Na/NFM-NFPP full cells (1.5–4.3 V, 0.1C, 25 °C) in commercial electrolyte; (e) The relationship between capacity and NFPP electrode added by the amount of NFM at 0.1C. (f) Normalization plot of the voltage - capacity curve of the first charge discharge cycle of the blended cathode (1.5–4.3 V).
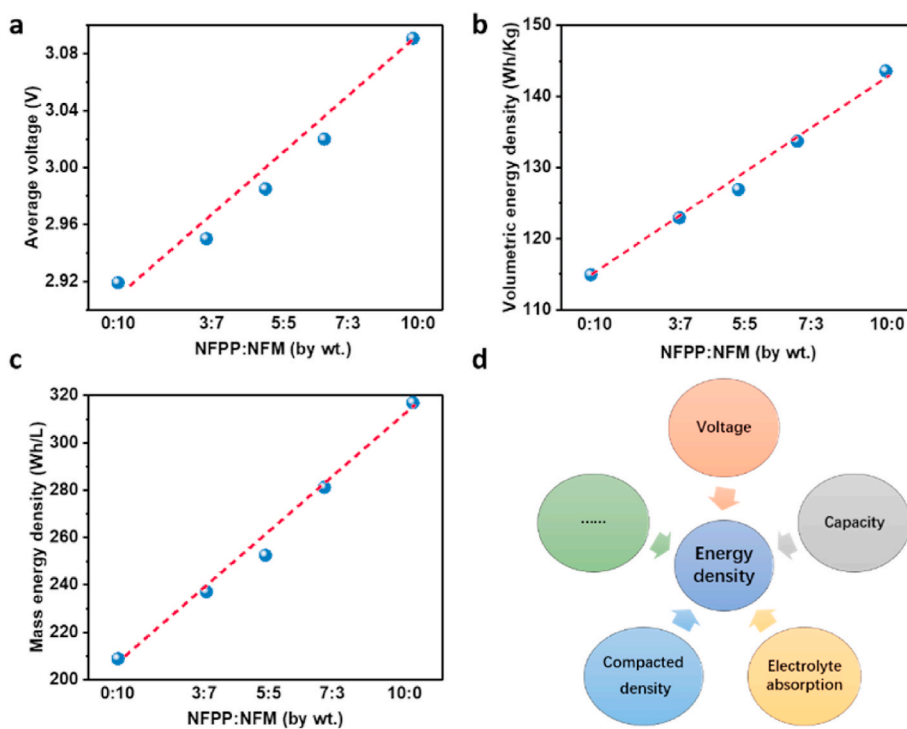


**Fig. 4.** The figure of energy density and the blended electrode of NFM-NFPP. The linear relationship diagram between (a) Average voltage, (b) Volumetric energy density, (c) Mass energy density, and the blending proportions of NFM-NFPP; (d) Schematic diagram of influencing factors of energy density.
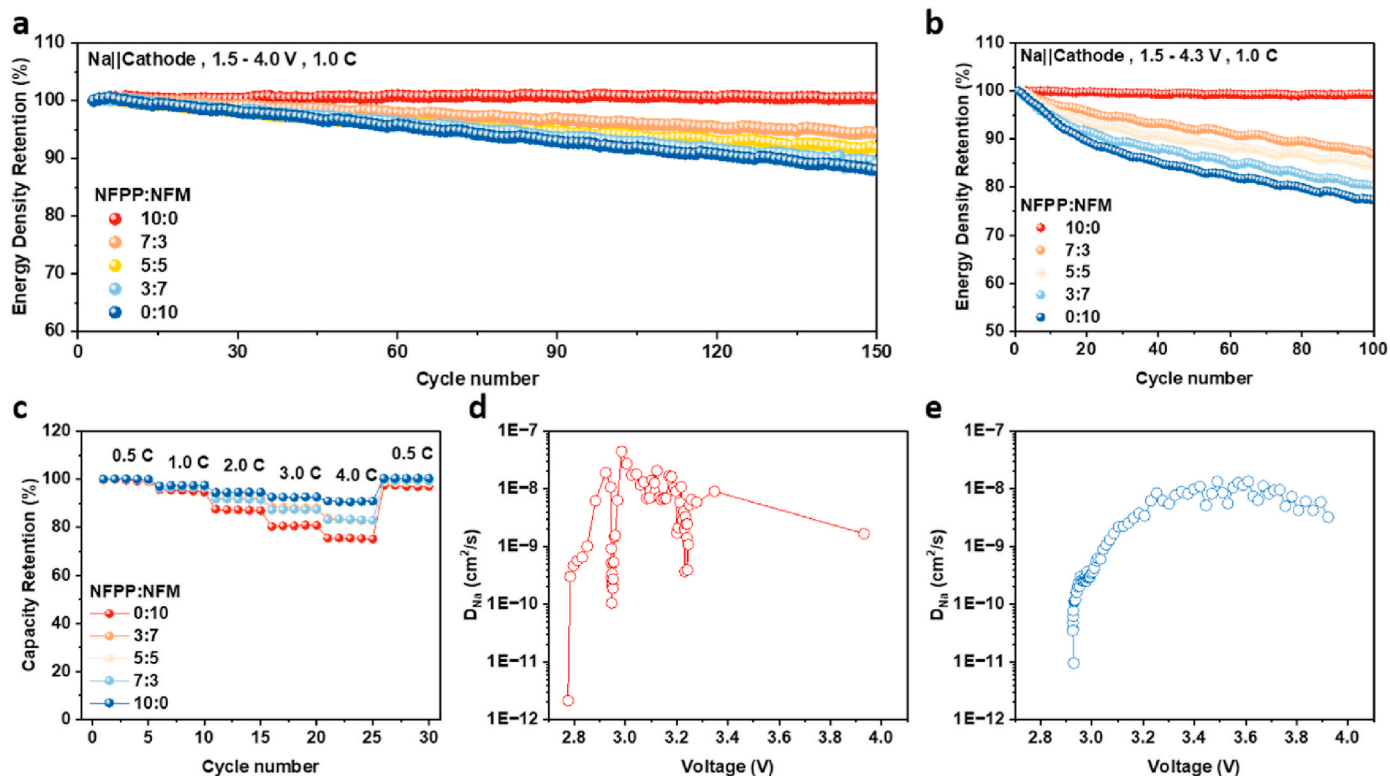
**Fig. 5.** Cycling and kinetic performance of NFM-NFPP electrode blended different proportions. Energy density retention rate with a voltage of (a)1.5–4.0 V, (b) 1.5−4.3 V; (c) Rate performance with a voltage of 1.5–4.0 V; The calculated Na + diffusion coefficients for desodiation process of (d) NFM and (e) NFPP.

particularly under high current densities (Fig. 5(c)). This enhancement is attributed to the faster Na ion diffusion of NFPP [35]. Therefore, the kinetic test of the charge process using GITT (Fig. 5(d, e) and Figs. S8 and S9) shows that NFM exhibits lower diffusion coefficients of $10^{-10}$ cm$^2$/s near 2.8 V, 3.0 V, and 3.2 V, while the diffusion coefficient of NFPP increases continuously during the charging process, and the diffusion coefficient of NFPP is higher throughout the charge process.

From the current researches touching on the battery safety, the exothermic behavior of the cathode materials is one of the main sources of heat during thermal runaway processes. Therefore, the study of the thermal stability of cathode materials is also an important part of battery application. Due to its structural instability, NFM is prone to phase transitions and the release of significant heat during the whole heating process [36]. In contrast, NFPP exhibits superior structural stability, maintaining its integrity and stability throughout the heating process [37]. Fig. 6(a) illustrates a pronounced exothermic peak for NFM near

300 °C, which indicates a significant thermal event. Upon the incorporation of NFPP, this exothermic peak diminishes progressively, with pure NFPP exhibiting substantially lower heat release compared to NFM. In addition, the heat release also increases with the increase of NFM, and a sudden increase occurs when the mass proportion of NFM reaches 50 % (Fig. 6(b)). By adjusting the ratio of NFM to NFPP, the heat release of the mixed electrode can be adjusted to a safer level, which will greatly reduce the safety hazards of the battery. In addition, in the research of LIBs, the active oxygen released by layered cathode materials will react violently with the electrolyte and lithiated graphite, which will provide a large amount of heat for thermal runaway [38]. Fortunately, through TG-MS testing, both NFPP and NFM showed no oxygen release behavior in the desodiation state, demonstrating high thermal stability (Fig. 6(c)).
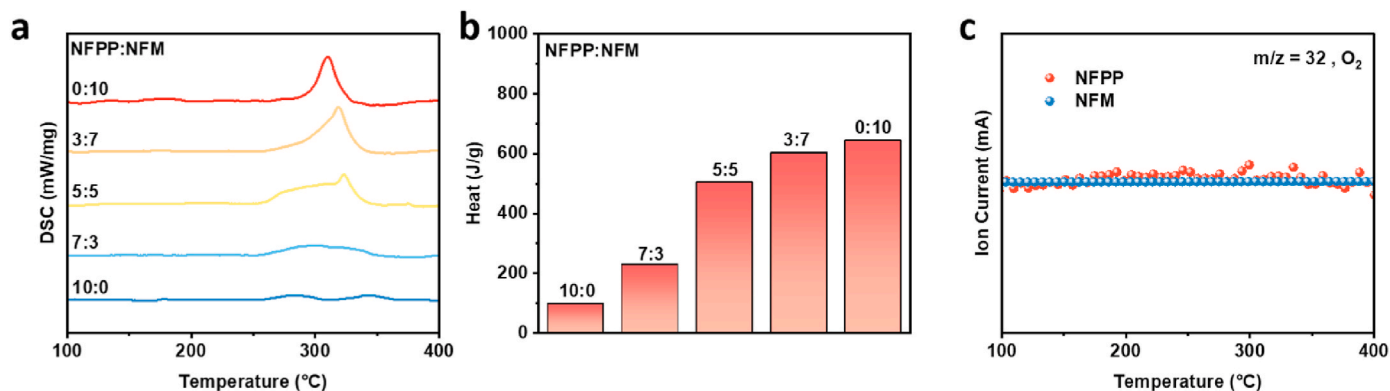


**Fig. 6.** The thermal behavior of NFM-NFPP blended electrode different proportions at 100 % SOC. (a, b) The DSC plots curve and heat release of NFM-NFPP electrodes blended different proportions in sealed crucibles; (c) The oxygen release from NFM or NFPP.

## 4. Conclusion

In this work, NFPP, NFM and their blended electrodes were used as a case model to systematically study the improvement of battery performance by blended electrodes from the aspects of electrode properties, electrochemical performance, and thermal stability. For NFPP cathode with lower specific capacity, the addition of NFM with high specific capacity will effectively enhance the discharge capacity of the cathode material. At the same time, it also has a forward effect on the average discharge voltage and compaction density of cathode materials. Therefore, the improvements of capacity, average discharge voltage, and compaction density can comprehensively enhance the energy density of batteries, which cannot be achieved solely through material modification. For NFM cathode with poor cycling stability and kinetic properties, the incorporation of NFPP into the blended electrode will slow down the capacity decay and improve the rate performance. In summary, active material blending is a simple and effective strategy to enhance the comprehensive performance of electrode/batteries, and may be a wiser and more strategic approach for the development of high-energy density batteries.

## CRediT authorship contribution statement

**Wei Li:** Writing – review & editing, Writing – original draft, Methodology, Investigation, Conceptualization. **Yuan Qin:** Writing – original draft, Methodology, Investigation, Conceptualization. **Shini Lin:** Validation, Data curation. **Honghao Xie:** Data curation. **Jing Zeng:** Writing – review & editing, Funding acquisition. **Peng Zhang:** Writing – review & editing. **Jinbao Zhao:** Writing – review & editing, Funding acquisition.

## Declaration of competing interest

The authors declare that they have no known competing financial interests or personal relationships that could have appeared to influence the work reported in this paper.

## Acknowledgements

## Appendix A. Supplementary data

Supplementary data to this article can be found online at https://doi.org/10.1016/j.jpowsour.2025.236275.

## Data availability

Data will be made available on request.

## References

[1] J.B. Goodenough, Y. Kim, Challenges for rechargeable Li batteries, Chem. Mater. 22 (2010) 587–603, https://doi.org/10.1021/cm901452z.

[2] X. Yu, A. Manthiram, Sustainable battery materials for next-generation electrical energy storage, Advanced Energy and Sustainability Research 2 (2021) 2000102, https://doi.org/10.1002/aesr.202000102.

[3] W. Li, H. Li, Z. He, W. Ji, J. Zeng, X. Li, Y. Zhang, P. Zhang, J. Zhao, Electrochemical failure results inevitable capacity degradation in Li-ion batteries—a review, Energies 15 (2022) 9165, https://doi.org/10.3390/en15239165.

[4] A. Rudola, R. Sayers, C.J. Wright, J. Barker, Opportunities for moderate-range electric vehicles using sustainable sodium-ion batteries, Nat. Energy 8 (2023) 215–218, https://doi.org/10.1038/s41560-023-01215-w.

[5] Y. Li, A. Vasileiadis, Q. Zhou, Y. Lu, Q. Meng, Y. Li, P. Ombrini, J. Zhao, Z. Chen, Y. Niu, X. Qi, F. Xie, R. van der Jagt, S. Ganapathy, M.-M. Titirici, H. Li, L. Chen, M. Wagemaker, Y.-S. Hu, Origin of fast charging in hard carbon anodes, Nat. Energy 9 (2024) 134–142, https://doi.org/10.1038/s41560-023-01414-5.

[6] T. Liu, Y. Zhang, Z. Jiang, X. Zeng, J. Ji, Z. Li, X. Gao, M. Sun, Z. Lin, M. Ling, J. Zheng, C. Liang, Exploring competitive features of stationary sodium ion batteries for electrochemical energy storage, Energy Environ. Sci. 12 (2019) 1512–1533, https://doi.org/10.1039/C8EE03727B.

[7] Y.-J. Guo, R.-X. Jin, M. Fan, W.-P. Wang, S. Xin, L.-J. Wan, Y.-G. Guo, Sodium layered oxide cathodes: properties, practicality and prospects, Chem. Soc. Rev. 53 (2024) 7828–7874, https://doi.org/10.1039/D4CS00415A.

[8] Q. Zhou, Y. Li, F. Tang, K. Li, X. Rong, Y. Lu, L. Chen, Y.-S. Hu, Thermal stability of high power 26650-type cylindrical Na-ion batteries, Chin. Phys. Lett. 38 (2021) 076501, https://doi.org/10.1088/0256-307X/38/7/076501.

[9] E.S. Zsoldos, D.T. Thompson, W. Black, S.M. Azam, J.R. Dahn, The operation window of lithium iron phosphate/graphite cells affects their lifetime, J. Electrochem. Soc. 171 (2024) 080527, https://doi.org/10.1149/1945-7111/ad6cbd.

[10] J.-Z. Guo, H.-X. Zhang, Z.-Y. Gu, M. Du, H.-Y. Lü, X.-X. Zhao, J.-L. Yang, W.-H. Li, S. Kang, W. Zou, X.-L. Wu, Heterogeneous NASICON-type composite as low-cost, high-performance cathode for sodium-ion batteries, Adv. Funct. Mater. 32 (2022) 2209482, https://doi.org/10.1002/adfm.202209482.

[11] J.-Y. Hwang, S.-T. Myung, Y.-K. Sun, Sodium-ion batteries: present and future, Chem. Soc. Rev. 46 (2017) 3529–3614, https://doi.org/10.1039/C6CS00776G.

[12] H. Yang, Q. Zhang, M. Chen, Y. Yang, J. Zhao, Unveiling the origin of air stability in polyanion and layered-oxide cathode materials for sodium-ion batteries and their practical application considerations, Adv. Funct. Mater. 34 (2024) 2308257, https://doi.org/10.1002/adfm.202308257.

[13] H.S. Hirsh, Y. Li, D.H.S. Tan, M. Zhang, E. Zhao, Y.S. Meng, Sodium-ion batteries paving the way for grid energy storage, Adv. Energy Mater. 10 (2020) 2001274, https://doi.org/10.1002/aenm.202001274.

[14] F. Ding, C. Zhao, D. Zhou, Q. Meng, D. Xiao, Q. Zhang, Y. Niu, Y. Li, X. Rong, Y. Lu, L. Chen, Y.-S. Hu, A novel Ni-rich O3-Na[Ni0.60Fe0.25Mn0.15]O2 cathode for Na-ion batteries, Energy Storage Mater. 30 (2020) 420–430, https://doi.org/10.1016/j.ensm.2020.05.013.

[15] C. Yang, S. Xin, L. Mai, Y. You, Materials design for high-safety sodium-ion battery, Adv. Energy Mater. 11 (2021) 2000974, https://doi.org/10.1002/aenm.202000974.

[16] Y. Cao, C. Yang, Y. Liu, X. Xia, D. Zhao, Y. Cao, H. Yang, J. Zhang, J. Lu, Y. Xia, A new polyanion Na$_3$Fe$_2$(PO$_4$)P$_2$O$_7$ cathode with high electrochemical performance for sodium-ion batteries, ACS Energy Lett. 5 (2020) 3788–3796, https://doi.org/10.1021/acsenergylett.0c01902.

[17] X. Wang, H. Li, W. Zhang, X. Ge, L. He, L. Zhang, S. Li, N. Wen, J. Guo, Y. Lai, S. Li, Z. Zhang, Unlocking fast and highly reversible sodium storage in Fe-based mixed polyanion cathodes for low-cost and high-performance sodium-ion batteries, J. Mater. Chem. A 11 (2023) 6978–6985, https://doi.org/10.1039/D3TA00014A.

[18] Y. Cao, C. Yang, Y. Liu, X. Xia, D. Zhao, Y. Cao, H. Yang, J. Zhang, J. Lu, Y. Xia, A new polyanion Na3Fe2(PO4)P2O7 cathode with high electrochemical performance for sodium-ion batteries, ACS Energy Lett. 5 (2020) 3788–3796, https://doi.org/10.1021/acsenergylett.0c01902.

[19] B. Zhang, G. Chen, Y. Yang, M. Liu, X. Li, H. Liu, Z.-F. Ma, Heterovalent chromium-doped Na3Fe2(PO4)P2O7 cathode material with superior rate and stability performance for sodium-ion storage, ACS Sustainable Chem. Eng. 11 (2023) 10083–10094, https://doi.org/10.1021/acssuschemeng.3c02013.

[20] S. Gao, Z. Zhu, H. Fang, K. Feng, J. Zhong, M. Hou, Y. Guo, F. Li, W. Zhang, Z. Ma, F. Li, Regulation of coordination chemistry for ultrastable layered oxide cathode materials of sodium-ion batteries, Adv. Mater. 36 (2024) 2311523, https://doi.org/10.1002/adma.202311523.

[21] C. Heubner, T. Liebmann, C. Lämmel, M. Schneider, A. Michaelis, Insights into the buffer effect observed in blended lithium insertion electrodes, J. Power Sources 363 (2017) 311–316, https://doi.org/10.1016/j.jpowsour.2017.07.108.

[22] C. Heubner, T. Liebmann, M. Schneider, A. Michaelis, Recent insights into the electrochemical behavior of blended lithium insertion cathodes: a review, Electrochim. Acta 269 (2018) 745–760, https://doi.org/10.1016/j.electacta.2018.02.165.

[23] Y. Zhang, D. Wang, C. Liang, Y. Han, Z. Li, Y. Huang, Design of double layer cathode electrode for improving the safety and stability of lithium-ion batteries, Chem. Eng. J. 495 (2024) 153344, https://doi.org/10.1016/j.cej.2024.153344.

[24] M. Yue, C. Aiken, J. Deshmukh, M.D.L. Garayt, M. Johnson, J.R. Dahn, C. Yang, Improved elevated temperature performance of LiFePO4/graphite cell by blending NMC640 in cathode, J. Electrochem. Soc. 170 (2023) 110532, https://doi.org/10.1149/1945-7111/ad0bab.

[25] D. Chatzogiannakis, V. Arszelewska, P.-E. Cabelguen, F. Fauth, M. Casas-Cabanas, M.R. Palacin, Understanding charge transfer dynamics in blended positive electrodes for Li-ion batteries, Energy Storage Mater. 69 (2024) 103414, https://doi.org/10.1016/j.ensm.2024.103414.

[26] T. Liebmann, C. Heubner, M. Schneider, A. Michaelis, Understanding kinetic and thermodynamic properties of blended cathode materials for lithium-ion batteries, Mater. Today Energy 22 (2021) 100845, https://doi.org/10.1016/j.mtener.2021.100845.

[27] T. Li, M. Lu, Y. Zhang, X. Xiang, S. Liu, C. Chen, Structural evolution and redox chemistry of robust ternary layered oxide cathode for sodium-ion batteries, J. Alloys Compd. 978 (2024) 173459, https://doi.org/10.1016/j.jallcom.2024.173459.

[28] X. Wu, G. Zhong, Y. Yang, Sol-gel synthesis of Na4Fe3(PO4)2(P2O7)/C nanocomposite for sodium ion batteries and new insights into microstructural evolution during sodium extraction, J. Power Sources 327 (2016) 666–674, https://doi.org/10.1016/j.jpowsour.2016.07.061.

[29] Y. Cao, X. Xia, Y. Liu, N. Wang, J. Zhang, D. Zhao, Y. Xia, Scalable synthesizing nanospherical Na4Fe3(PO4)2(P2O7) growing on MCNTs as a high-performance cathode material for sodium-ion batteries, J. Power Sources 461 (2020) 228130, https://doi.org/10.1016/j.jpowsour.2020.228130.

[30] H. Yang, X. Kong, J. Li, P. Dai, J. Zeng, Y. Yang, J. Zhao, In-situ construction of a thermodynamically stabilized interface on the surface of single crystalline Ni-rich cathode materials via a one-step molten-salt route, Nano Res. (2022) 1–9, https://doi.org/10.1007/s12274-022-4768-6.

[31] F. Li, L. Kong, Y. Sun, Y. Jin, P. Hou, Micron-sized monocrystalline LiNi1/3Co1/3Mn1/3O2 as high-volumetric-energy-density cathode for lithium-ion batteries, J. Mater. Chem. A 6 (2018) 12344–12352, https://doi.org/10.1039/C8TA03363C.

[32] U.-H. Kim, L.-Y. Kuo, P. Kaghazchi, C.S. Yoon, Y.-K. Sun, Quaternary layered Ni-rich NCMA cathode for lithium-ion batteries, ACS Energy Lett. 4 (2019) 576–582, https://doi.org/10.1021/acsenergylett.8b02499.

[33] Y. Duan, B. Zhang, J. Zheng, J. Hu, J. Wen, D.J. Miller, P. Yan, T. Liu, H. Guo, W. Li, X. Song, Z. Zhuo, C. Liu, H. Tang, R. Tan, Z. Chen, Y. Ren, Y. Lin, W. Yang, C.-M. Wang, L.-W. Wang, J. Lu, K. Amine, F. Pan, Excess Li-ion storage on reconstructed surfaces of nanocrystals to boost battery performance, Nano Lett. 17 (2017) 6018–6026, https://doi.org/10.1021/acs.nanolett.7b02315.

[34] J. Hu, X. Li, Q. Liang, L. Xu, C. Ding, Y. Liu, Y. Gao, Optimization strategies of Na3V2(PO4)3 cathode materials for sodium-ion batteries, Nano-Micro Lett. 17 (2024) 33, https://doi.org/10.1007/s40820-024-01526-x.

[35] M. Chen, W. Hua, J. Xiao, D. Cortie, W. Chen, E. Wang, Z. Hu, Q. Gu, X. Wang, S. Indris, S.-L. Chou, S.-X. Dou, NASICON-type air-stable and all-climate cathode for sodium-ion batteries with low cost and high-power density, Nat. Commun. 10 (2019) 1480, https://doi.org/10.1038/s41467-019-09170-5.

[36] Y. Xie, G.-L. Xu, H. Che, H. Wang, K. Yang, X. Yang, F. Guo, Y. Ren, Z. Chen, K. Amine, Z.-F. Ma, Probing thermal and chemical stability of NaxNi1/3Fe1/3Mn1/3O2 cathode material toward safe sodium-ion batteries, Chem. Mater. 30 (2018) 4909–4918, https://doi.org/10.1021/acs.chemmater.8b00047.

[37] T. Jin, H. Li, K. Zhu, P.-F. Wang, P. Liu, L. Jiao, Polyanion-type cathode materials for sodium-ion batteries, Chem. Soc. Rev. 49 (2020) 2342–2377, https://doi.org/10.1039/C9CS00846B.

[38] J. Hou, X. Feng, L. Wang, X. Liu, A. Ohma, L. Lu, D. Ren, W. Huang, Y. Li, M. Yi, Y. Wang, J. Ren, Z. Meng, Z. Chu, G.-L. Xu, K. Amine, X. He, H. Wang, Y. Nitta, M. Ouyang, Unlocking the self-supported thermal runaway of high-energy lithium-ion batteries, Energy Storage Mater. 39 (2021) 395–402, https://doi.org/10.1016/j.ensm.2021.04.035.